Modeling of Thermoacoustic Resonators With Nonuniform Medium and Boundary Conditions

Konstantin I. Matveev[1]
e-mail: matveev@wsu.edu

Sungmin Jung

School of Mechanical and Materials Engineering,
Washington State University,
Pullman, WA 99164-2920

The subject of this paper is modeling of low-amplitude acoustic fields in enclosures with nonuniform medium and boundary conditions. An efficient calculation method is developed for this class of problems. Boundary conditions, accounting for the boundary-layer losses and movable walls, are applied near solid surfaces. The lossless acoustic wave equation for a nonuniform medium is solved in the bulk of the resonator by a finite-difference method. One application of this model is for designing small thermoacoustic engines. Thermoacoustic processes in the regular-geometry porous medium inserted in resonators can be modeled analytically. A calculation example is presented for a small-scale thermoacoustic engine coupled with an oscillator on a flexing wall of the resonator. The oscillator can be used for extracting mechanical power from the engine. A nonuniform wall deflection may result in a complicated acoustic field in the resonator. This leads to across-the-stack variations of the generated acoustic power and local efficiency of thermoacoustic energy conversion. [DOI: 10.1115/1.4003200]

Keywords: thermoacoustic engine, energy conversion, acoustic resonator, nonuniform media, linear acoustics

1 Introduction

Modeling of acoustic field in enclosures, such as mufflers, rooms, and thermoacoustic devices, is an important engineering problem. Complete modeling of sound including damping mechanisms in the entire fluid domain is computationally expensive. When dissipation is not important and the sound amplitude is small, a simplified form of the linearized wave equation can be easily solved by various techniques, such as boundary element methods. In many acoustic systems, losses are important only in acoustic boundary layers formed near solid surfaces. Then, using wall admittances [1,2] or thermoviscous functions [3], it is possible to account for this damping while neglecting thermoviscous effects outside boundary layers.

Unsteady heat release in acoustic resonators can lead to sound generation or attenuation. Thermoacoustic engines represent novel devices where acoustic power is produced from heat without involving movable solid parts [4]. The acoustic power is usually generated inside a porous material known as a stack, which is subjected to a temperature gradient. A schematic of a classical quarter-wavelength thermoacoustic engine is shown in Fig. 1. The generated acoustic power can be used for cooling applications, electricity production, and gas mixture separation. Calculations of thermoacoustic engines often rely on using thermoviscous functions to predict gain or loss of acoustic power in the system elements. For example, modeling of acoustic field in ducts by the thermoacoustic code DELTAE [5] is based on the assumption that acoustic pressure and mean temperature are uniform across in the duct cross sections, and the solution of a quasi-one-dimensional wave equation is obtained using thermoviscous functions that account for the wall effects.

In recent years, efforts have been undertaken to develop small-scale thermoacoustic engines that can be used as elements of portable electric power generators [6,7]. The produced sound energy can be harnessed by electroacoustic transformers (Fig. 1(*b*)), such as piezomembranes. These membranes create nonuniform boundary conditions at the resonator walls and significantly distort the one-dimensionality of acoustic field in resonators, especially in enclosures with large cross-sectional areas, which are beneficial for reducing wall losses. Also, heat sources/sinks in miniature systems are placed (possibly asymmetrically) outside resonators, and heat is delivered/removed to/from the stack ends via conduction through porous materials, such as wire mesh or end sections of the stack. With less effective heat exchangers and wider resonators, transverse variations of the mean temperature may become significant and affect the acoustic field. These transverse nonuniformities make commonly used calculation methods (such as DELTAE) inapplicable for acoustic modeling of resonators in miniature thermoacoustic systems.

In the present paper, an efficient computational method addressing this problem is developed. The appropriate boundary conditions are applied near the resonator boundaries, accounting for the boundary-layer losses, movable walls, and thermoacoustic stack interfaces. The lossless linearized acoustic wave equation is solved in the bulk of the resonator (filled with a nonuniform fluid) by a finite-difference method. Although the focus of this study is on thermoacoustic engines, the discussed method can be applied for other acoustic problems with lossy resonators.

2 Mathematical Model

Steady-state, low-amplitude, single-frequency acoustic oscillations are considered inside a resonator. The pressure and velocity can be presented as follows [4]:

$$p(\underline{x},t) = p_m + \mathrm{Re}[p_1(\underline{x})e^{i\omega t}] \tag{1}$$

$$\underline{u}(\underline{x},t) = \mathrm{Re}[\underline{u}_1(\underline{x})e^{i\omega t}] \tag{2}$$

where p_m is the mean pressure, p_1 and $\underline{u}_1$ are the complex amplitudes of acoustic pressure and velocity, respectively, ω is the radian frequency, t is the time, and i is the imaginary unity. The acoustic streaming is ignored in the present study due to consideration of only low-amplitude sound. The acoustic streaming is a second-order effect with respect to the acoustic pressure amplitude. The streaming usually becomes important when the ratio

[1]Corresponding author.

Contributed by the Technical Committee on Vibration and Sound of ASME for publication in the JOURNAL OF VIBRATION AND ACOUSTICS. Manuscript received April 30, 2010; final manuscript received September 7, 2010; published online March 31, 2011. Assoc. Editor: Liang-Wu Cai.

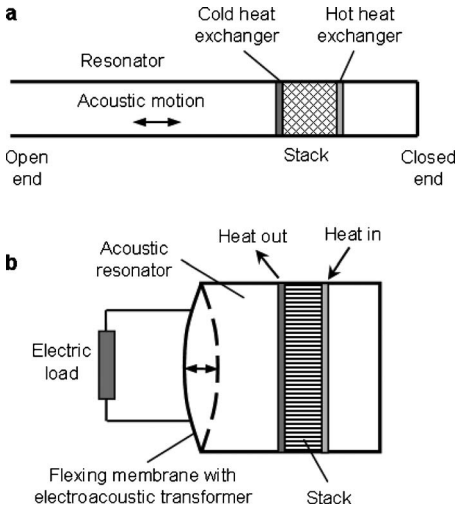

Fig. 1 Schematics of (*a*) classical standing-wave thermoacoustic engine and (*b*) low-aspect-ratio engine with electroacoustic transformer

p_1/p_m exceeds about 5% [4,8]. In all examples presented in this paper, the relative pressure amplitudes are smaller than 2%, with an exception of one special case with larger amplitudes.

Thermoviscous losses are considered to be negligible far from the walls of the resonator. Therefore, the acoustic pressure field satisfies a modified Helmholtz equation for a nonuniform medium, which can be obtained from the linear acoustic theory [9],

$$\nabla^2 p_1 + \frac{\omega^2}{a^2} p_1 - \frac{1}{\rho} \nabla p_1 \cdot \nabla \rho = 0 \tag{3}$$

where a and ρ are the local speed of sound and density, respectively. The last term in Eq. (3) is responsible for a nonuniformity of gas density inside a resonator, which can be caused, for example, by a spatially variable mean temperature field. It is assumed that acoustic losses in the bulk of resonator are much smaller than those at the walls.

To account for thermoviscous losses at the resonator solid walls and possible normal oscillations of the walls, a boundary condition can be introduced for the amplitude u_1 of the acoustic velocity normal to the wall and evaluated at the outer edge of the acoustic boundary layer. This condition follows from the acoustic momentum equation,

$$i\rho\omega u_1 = i\rho\omega(u_\delta + u_w) = -\frac{\partial p_1}{\partial \zeta} \tag{4}$$

where ζ is the coordinate normal to the wall, u_δ is the amplitude of the velocity due to thermoviscous effects in the acoustic boundary layer, and u_w is the velocity amplitude of the wall oscillations (Fig. 2(*b*)). In a nonuniform medium, the expression for velocity u_δ can be determined from results of Olson and Swift [10],

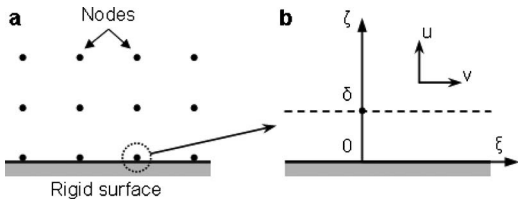

Fig. 2 (*a*) Part of numerical grid. (*b*) Magnified view of a zone near rigid surface.

$$u_\delta = \frac{\sqrt{i\upsilon}}{\rho\omega^{3/2}} \frac{\partial^2 p_1}{\partial \xi^2} - \frac{\sqrt{i\omega\chi}}{\rho a^2}(\gamma - 1)p_1 + \frac{\sqrt{i}}{\rho^2\omega^{3/2}} \left[\left(\frac{\sqrt{\upsilon} - \sqrt{\chi}}{1 - \sigma} - \sqrt{\upsilon} \right) \frac{\partial \rho}{\partial \xi} + \frac{\rho}{2\sqrt{\upsilon}} \frac{\partial \upsilon}{\partial \xi} \right] \frac{\partial p_1}{\partial \xi} \tag{5}$$

where ξ is the coordinate parallel to the wall, υ is the gas kinematic viscosity, χ is the thermal diffusivity, γ is the specific heat ratio, and σ is the Prandtl number.

The acoustic field in a resonator with a given mean temperature field can be calculated by a finite-difference method. The numerical grid size is selected to be much greater than the acoustic boundary-layer thickness δ, which can be estimated as follows:

$$\delta \sim \max(\delta_\upsilon; \delta_k) = \max\left(\sqrt{\frac{2\upsilon}{\omega}}; \sqrt{\frac{2\chi}{\omega}} \right) \tag{6}$$

where δ_υ and δ_k are the viscous and thermal penetration depths, respectively. For solving Eq. (3) in the bulk of the resonator, the boundary points of the numerical mesh can be approximately placed at the wall surface due to smallness of δ in comparison with a computational cell size (Fig. 2(*a*)). The boundary condition in the form of Eq. (4) can be applied at these points. At the other points (in the bulk of a resonator), Eq. (3) is used. Discretized forms of Eqs. (3) and (4) form a system of linear algebraic equations for the acoustic pressure amplitude. Once the pressure field is determined, the acoustic velocity in the bulk of a resonator can be found from the acoustic momentum equation,

$$i\omega u_1 = -\nabla p_1 \tag{7}$$

If a porous material (called "stack" in thermoacoustics) is inserted inside a resonator, then a modified wave equation must be solved inside this medium since viscous and thermal relaxation effects will be important in the entire gas volume in the stack. This equation was derived by Swift [4] for regular stacks with a longitudinal-pore structure,

$$[1 + (\gamma - 1)f_k]p_1 + \frac{\gamma p_m}{\omega^2} \frac{d}{dx}\left(\frac{1 - f_\upsilon}{\rho} \frac{dp_1}{dx} \right) - \frac{a^2}{\omega^2} \frac{f_k - f_\upsilon}{1 - \sigma} \frac{1}{T} \frac{dT}{dx} \frac{dp_1}{dx} = 0 \tag{8}$$

where x is the coordinate along pores in the stack, T is the time-average temperature in the pore section, and f_υ and f_k are the thermoacoustic functions specific to the stack pore geometry. In this analysis, the temperature distribution in the stack is treated as a given condition, and no heat exchangers are included into consideration. For a stack composed of parallel plates, thermoacoustic functions are given as follows [4]:

$$f_{k,\upsilon} = \frac{\tanh[(1 + i)y_0/\delta_{k,\upsilon}]}{(1 + i)y_0/\delta_{k,\upsilon}} \tag{9}$$

where y_0 is a half of the spacing between neighboring plates, and penetration depths δ_k and δ_υ are given in Eq. (6). The acoustic velocity component along the pore, averaged over the pore cross section, is related to the acoustic pressure gradient,

$$\langle u_1 \rangle = i \frac{1 - f_\upsilon}{\rho\omega} \frac{dp_1}{dx} \tag{10}$$

It is assumed that at the stack-resonator interface the acoustic pressure is continuous, while the acoustic velocity experience a jump due to a slight variation of the cross-sectional area for oscillating gas flow in the stack,

$$p_1|_{x=L_1-} = p_1|_{x=L_1+}, \quad p_1|_{x=L_2-} = p_1|_{x=L_2+} \tag{11}$$

$$u_1|_{x=L_1-} = \varphi\langle u_1 \rangle|_{x=L_1+}, \quad u_1|_{x=L_2+} = \varphi\langle u_1 \rangle|_{x=L_2-} \tag{12}$$

where L_1 and L_2 are the coordinates of the stack ends (Fig. 3(*a*)) and φ is the stack porosity (close to 1). The acoustic pressure and velocity may vary at the stack end planes. Equations (11) and (12)

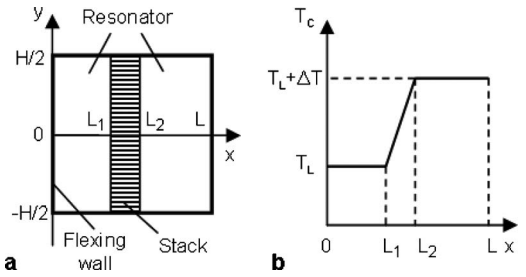

Fig. 3 (*a*) Geometry of a 2D thermoacoustic engine with flexing wall on the left boundary. (*b*) Given mean temperature profile at *y*=0.

represent simplified forms of the joining conditions. At large acoustic amplitudes or low-porous stacks, the joining conditions would require more complicated correction factors due to complex thermal and acoustic processes at the interfaces [4,11].

The coupling between the gas oscillating in a resonator and a vibrating wall implies a relation between amplitudes of the wall velocity u_w and the local acoustic pressure p_1. In general, this relation depends on the structural properties of the flexing wall. Since in this study we are concerned mainly with fluid oscillations in the resonator, an idealized linear mechanical oscillator model is adopted for a flexing part of the wall. In such an oscillator, its effective velocity amplitude U_1 is coupled to the force amplitude F_1 as follows:

$$U_1 = \frac{i\omega F_1}{K - \omega^2 M + i\omega R} \tag{13}$$

where K and M are the stiffness and mass of an oscillator, $U_1 = 1/A\int_A u_w dA$ is the area-averaged velocity amplitude at the flexing wall surface, and A is the surface area. For simplicity, it is assumed that there is no internal damping in the oscillator, so a real-valued coefficient R in Eq. (13) is responsible only for harnessing the mechanical power of the oscillator by external means. In practical applications this power can be further converted in other energy forms, such as electricity. The effective force in Eq. (13) is defined as follows:

$$F_1 = -\frac{1}{\tilde{U}_1}\int_A p_1 \tilde{u}_w dA \tag{14}$$

where the tilde stands for a complex conjugate and the minus sign corresponds to the x-axis directed from the flexing wall into the resonator as in Fig. 3(a). The form of Eq. (14) ensures that the time-averaged acoustic power consumed by the flexing wall is completely extracted from the oscillator. This power can be calculated via acoustic variables (for geometry in Fig. 3) or mechanical parameters,

$$P = -\frac{1}{2}\mathrm{Re}\left[\int_A p_1 \tilde{u}_w dA\right] = \frac{1}{2}\mathrm{Re}[F_1 \tilde{U}_1]$$

$$= \frac{|F_1|^2}{2}\frac{R}{(\omega_0^2/\omega^2 - 1)^2 \omega^2 M^2 + R^2} \tag{15}$$

where $\omega_0 = \sqrt{K/M}$ is the natural frequency of the oscillator. If $R = 0$, then no acoustic power is delivered to the flexing wall and no mechanical power is taken from the engine.

3 Results

The mathematical model is first validated for a constant-temperature resonator. The resonator geometry is similar to that shown in Fig. 3(a), but with no stack present, and the left wall oscillates in a uniform, pistonlike motion with the velocity amplitude $u_w = 3$ m/s at the half-resonance frequency. The 2 cm $\times 2$ cm two-dimensional resonator is filled with 5 bar air at a constant mean temperature of 400 K. The top and bottom boundaries are isothermal, while the left and right boundaries are adiabatic. The analytical solutions for the acoustic pressure and velocity amplitudes averaged over the cross-sectional areas are given as follows [9]:

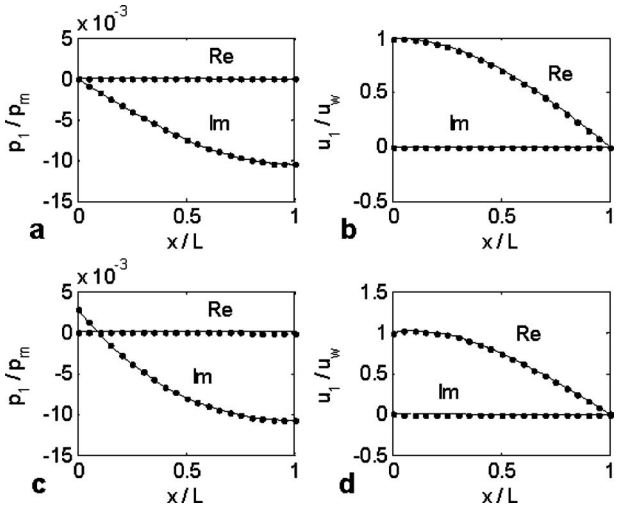

Fig. 4 Model validation results. (*a*) Constant-temperature lossy resonator. Solid lines, analytical solution; points, 2D numerical solution. (*b*) Resonator with linear temperature variation. Solid lines, solution of 1D wave equation with thermoviscous functions (Eq. (8)); points, 2D numerical solution. Re and Im symbols indicate the real and imaginary parts of solutions, respectively.

$$p_1(x) = A_1 \exp(-ikx) + B_1 \exp(ikx) \tag{16}$$

$$u_1(x) = \frac{A_1}{Z}\exp(-ikx) - \frac{B_1}{Z}\exp(ikx) \tag{17}$$

where k and Z are the wavenumber and the specific acoustic impedance, respectively. In a two-dimensional duct, they can be expressed via thermoviscous functions (Eq. (9)) with $H/2$ substituted for y_0,

$$k = \frac{\omega}{a}\sqrt{\frac{1 + (\gamma - 1)f_k}{1 - f_v}} \tag{18}$$

$$Z = \frac{\rho a}{\sqrt{(1 - f_v)[1 + (\gamma - 1)f_k]}} \tag{19}$$

Constants A_1 and B_1 in Eqs. (16) and (17) are found from two boundary conditions, $u_1(0) = u_w$ and $u_1(L) = 0$. A comparison between the analytical solution and the two-dimensional numerical solution by the method developed here is shown in Figs. 4(a) and 4(b).

Another validation has been carried out for the same system but with a linear variation of mean temperature along the resonator, so that the left and right walls are at 200 K and 600 K, respectively. While the analytical solution is not possible for this case, a numerical solution of the one-dimensional wave equation (Eq. (8)) can be easily found using thermoviscous functions (Eq. (9)). (A similar approach is implemented in the DELTAE algorithm for resonators.) The comparison between our 2D model and a solution of 1D wave equation is given in Figs. 4(c) and 4(d). The agreement between the results of the 2D model developed here and other solutions is good.

Upon validation, the method described in Sec. 2 has been applied to model a small-scale two-dimensional thermoacoustic engine with a flexing wall. The oscillating boundary can be used to

Table 1 Specifications of thermoacoustic engine

Length	$L=2$ cm
Height	$H=2$ cm
Left position of the stack	$L_1=5$ mm
Right position of the stack	$L_2=10$ mm
Stack porosity	$\varphi=0.95$
Gas type	Air
Mean pressure	$p_m=5$ bars
Mean temperature of the cold part	$T_L=300$ K
Transverse temperature difference	$\Delta T_y=20$ K

extract mechanical power from the engine. A system schematic is shown in Fig. 3(*a*), and main parameters are listed in Table 1. One advantage of this low-aspect-ratio configuration in comparison with common high-aspect-ratio engines is the reduced surface area of the resonator, which results in decreased acoustic attenuation at the walls. Additionally, if the operational frequency of the engine is sufficiently smaller than the natural frequency of the resonator, then the wall losses will be further reduced, since thermoviscous damping decreases with decreasing frequency. This can be achieved if the natural frequency of the flexing wall is selected to be much smaller than the resonator natural frequency.

There are two main modeling complications arising in this configuration. First, due to a nonuniform deflection of the flexing wall, the acoustic field in the direction transverse to dominant acoustic motions can also have significant nonuniformity. Second, the mean temperature may vary with the y-coordinate since uniform delivery/extraction of heat to/from the stack is difficult to achieve in low-aspect-ratio small-scale systems. Previously used thermoacoustic calculation tools (applied mainly for large systems) do not address these problems. However, the method presented in this paper can handle both effects. In this analysis, the mean temperature field and a form of the movable wall deflection are treated as given inputs since the focus of this study is on solving the acoustic problem. In a complete analysis, additional models for heat transfer and wall deformation will have to be introduced and coupled with the acoustic model.

In the presented calculation example, a simple but realistic form of the mean temperature field is given as follows:

$$T(x,y)=\begin{cases} T_L+\Delta T_y y/H, x<L_1 \\ T_L+\Delta T(x-L_1)/(L_2-L_1)+\Delta T_y y/H, L_1<x<L_2 \\ T_L+\Delta T+\Delta T_y y/H, x>L_2 \end{cases} \tag{20}$$

where L and H are the length and width of the resonator, respectively, T_L is the mean temperature of the cold part of the resonator, and $\Delta T>0$ is a constant temperature difference between the stack ends along the x-coordinate. The center-plane ($y=0$) mean temperature profile is shown in Fig. 3(*b*). ΔT_y is a constant temperature difference between the upper ($y=H/2$) and lower ($y=-H/2$) walls of the resonator. In the present example, a moderate transverse temperature difference of 20 K is chosen (Table 1), corresponding to realistic temperature nonuniformity estimated for one particular system setup. However, the present mathematical model can handle any ΔT_y, and practical systems with larger ΔT_y are also possible.

It is assumed that the flexing wall located at $x=0$ deforms as a cosine function of y, so its velocity amplitude (as well as the gas velocity amplitude at the wall surface) is given by the following expression:

$$u_w(y)=U_w\cos\left(\frac{\pi y}{H}\right) \tag{21}$$

where U_w is the wall velocity amplitude at $y=0$. The end points of this wall are fixed, and the maximum velocity (and deflection) is achieved in the middle of the wall. The velocity of the flexing wall described by Eq. (21) is an idealization. The actual velocity distribution in real devices will depend on the properties of the wall, fluid, resonator geometry, and temperature field. The other walls in the considered system, located at $y=H/2$, $y=-H/2$, and $x=L$, do not move at all.

One of the most important characteristics of thermoacoustic engines is the critical temperature difference between the stack ends ΔT_{cr}, which corresponds to the onset of sound. This threshold is calculated for the system with parameters given in Table 1. The parallel-plate stack is considered with a half-spacing between plates taken as $y_0=1.3\delta_k$, where δ_k is the thermal penetration length defined in Eq. (6). The wall oscillator mass M and its natural frequency $f_0=\omega_0/2\pi$ are treated as variable parameters. The number of computational nodes in each direction of the domain is selected to be $n=21$. (It was found that in a mesh with twice smaller cell size a change in results is usually less than 1%.) The wave equations in the resonator and stack (Eqs. (3) and (8)) are solved together with the boundary conditions (Eqs. (4), (11), and (12)) by the second-order finite-difference scheme. The frequency of acoustic oscillations f is the eigenvalue in this problem. This frequency and the critical temperature difference are found iteratively by ensuring that the power extraction coefficient R in Eqs. (13) and (15) is zero at the sound onset.

The calculated values of ΔT_{cr} and f for various oscillator parameters M and f_0 are shown in Fig. 5. In this figure, the resonator natural frequency f_r is estimated as for a half-wavelength uniform resonator, i.e., $f_r=a/2L$, where a is the mean speed of sound. This frequency is not close to the frequency of acoustic oscillations due to the presence of a flexing wall oscillator at the left boundary. The mass of the gas in the resonator M_g (per unit length in a two-dimensional problem) and the resonator natural frequency f_r are in the ranges of 1.64–2.13 g/m and 9.08–10.6 kHz, respectively, for corresponding temperature conditions. The normalized critical temperature difference shown in Fig. 5(*b*) is defined according to Swift [4],

$$\Gamma=\frac{\Delta T_{cr}}{\Delta T_{cr,id}}=\Delta T_{cr}\frac{\rho c_p|\langle u_1\rangle|}{\omega L_s|p_1|} \tag{22}$$

where $L_s=L_2-L_1$ is the stack length, and the gas properties and acoustic amplitudes are evaluated as mean values at the stack middle section $x=(L_1+L_2)/2$. The ideal critical temperature gradient $|\nabla T_{cr,id}|=\Delta T_{cr,id}/L_s$ corresponds to a single plate placed in an inviscid fluid that acoustically oscillates with a standing-wave phasing.

From the results in Fig. 5(*a*), one can see that selecting a low natural frequency and a large mass of an oscillator (at fixed values of other system parameters) is favorable for reducing the critical temperature difference. At a higher ratio of the natural frequencies of an oscillator and resonator, ΔT_{cr} increases and its sensitivity to the oscillator mass decreases.

Similar to the behavior of ΔT_{cr}, the frequency of self-excited acoustic oscillations f decreases with decreasing the natural frequency of the oscillator and increasing mass (Fig. 5(*c*)). This leads to the reduction of thermoviscous losses and earlier sound onset (lower ΔT_{cr}). The frequency of oscillations is always higher than the oscillator natural frequency f_0 in the studied range of the system parameters (Fig. 5(*d*)), but it approaches f_0 when the ratio f_0/f_r increases. As f_0 (or oscillator stiffness K) approaches zero, f stabilizes at a certain level which depends on the oscillator mass (Fig. 5(*c*)). The role of stiffness in this limit is played by a compressibility of the gas inside resonator.

An example of calculated acoustic pressure and x-component of the velocity is given in Fig. 6. The system parameters are the same as those given in Table 1 and described by Eqs. (20) and (21). Additionally, several other parameters are fixed as follows: the stack plate half-spacing $y_0=5\times10^{-5}$ m, the natural frequency of the oscillator $f_0=450$ Hz, the oscillator mass $M=10$ g/m, the

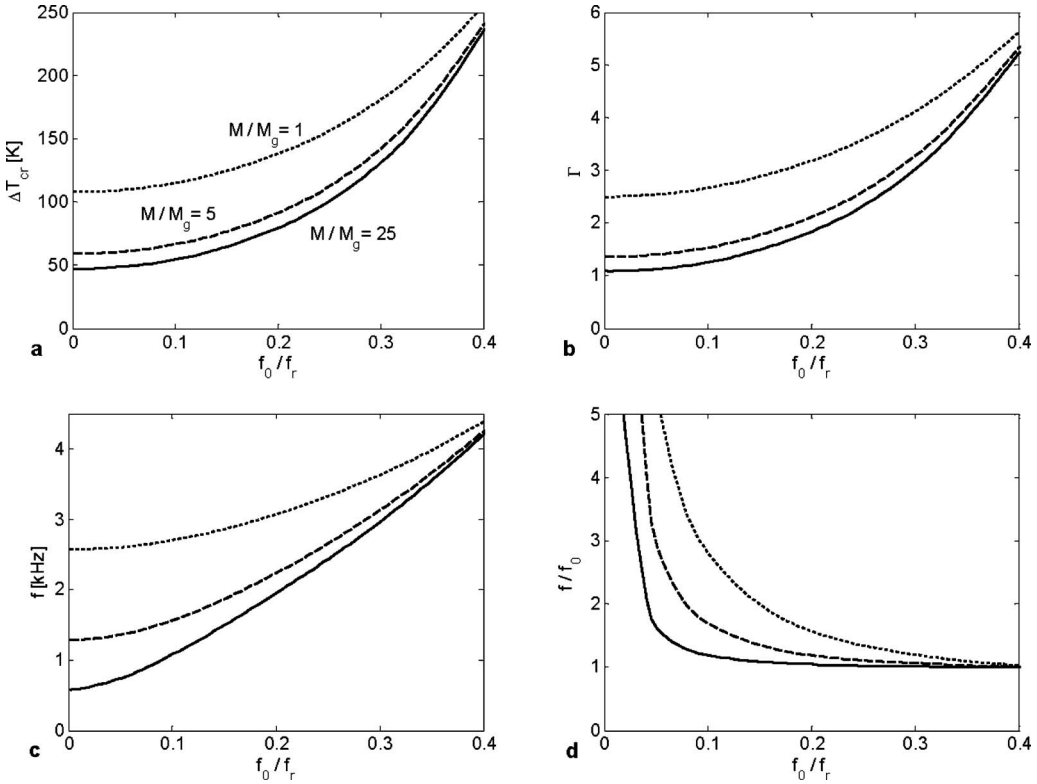

Fig. 5 ((*a*) and (*b*)) **Dimensional and normalized critical temperature difference.** ((*c*) and (*d*)) **Dimensional and normalized frequency of the engine at the sound onset. Solid line, M/M_g=25; dashed line, M/M_g=5; dotted line, M/M_g=1.**

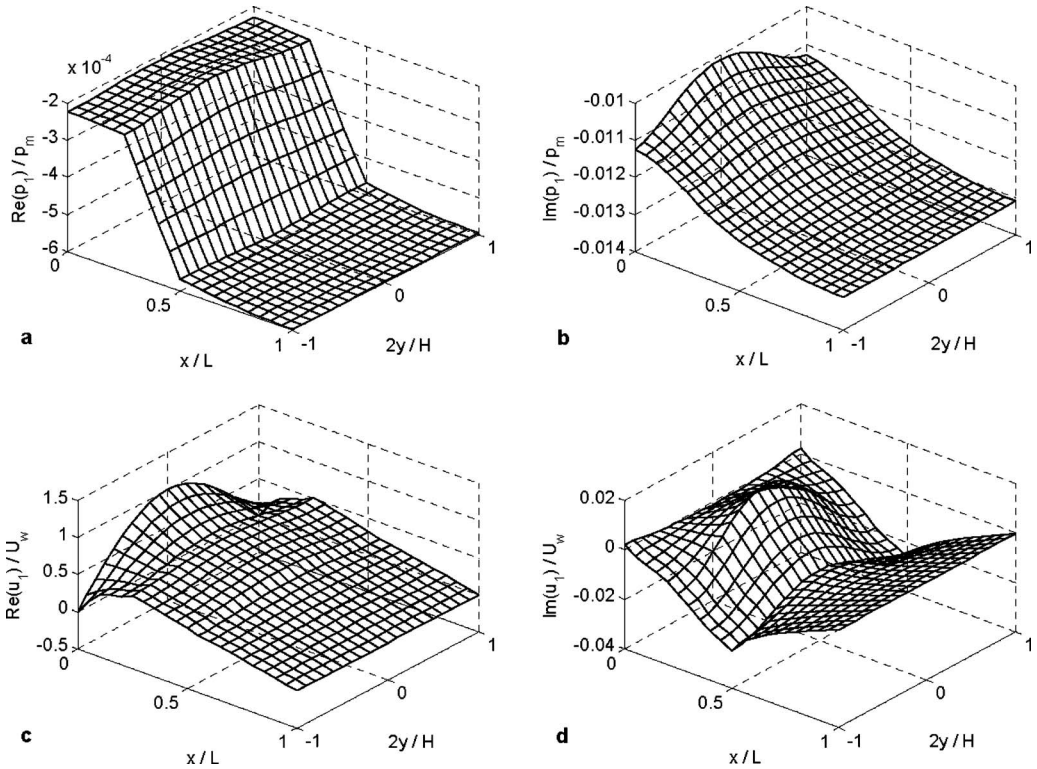

Fig. 6 Complex amplitudes of ((*a*) and (*b*)) **acoustic pressure normalized by mean pressure and** ((*c*) and (*d*)) **x-component of acoustic velocity normalized by maximum velocity at flexing wall. Velocities inside stack are averaged over pore cross sections.**

stack temperature difference $\Delta T = 100$ K (which is above the corresponding critical temperature difference), and the maximum wall velocity amplitude $U_w = 3$ m/s.

As shown in Fig. 6, the real component of the acoustic velocity (Fig. 6(*c*)) and the imaginary component of the acoustic pressure (Fig. 6(*b*)) dominate the imaginary velocity (Fig. 6(*d*)) and the real pressure (Fig. 6(*a*)), respectively. This indicates that the principal acoustic motions occur in the standing-wave phasing, where the acoustic pressure and velocity are shifted by about 90 deg. However, since the other components of the acoustic pressure and velocity are not zero (Figs. 6(*a*) and 6(*d*)), the phase shift is not exactly 90 degrees. This implies that some acoustic energy is transported through the system since the time-averaged acoustic energy flux is proportional to $\mathrm{Re}(p_1\tilde{u}_1)$.

Although the dominant acoustic motions occur along the *x*-coordinate, acoustic variables also depend on the *y*-coordinate outside the boundary layers. The nonuniform motions of the flexing wall cause a strong variability of the real component of the acoustic velocity at this wall boundary (Fig. 6(*c*)). This variability disappears on the opposite stationary wall since the velocity approaches zero. The focusing of the imaginary acoustic pressure at the center of the flexing wall (Fig. 6(*b*)) and the imaginary velocity in the central portion of the stack (Fig. 6(*d*)) are also noticeable.

The variation of acoustic field in the direction perpendicular to the main acoustic oscillations leads to nonuniform thermoacoustic energy conversion in the stack. The flux of generated acoustic energy out of the stack, its normalized value, and the local stack-based thermoacoustic efficiency for the considered here geometry can be defined as follows:

$$W(y) = \tfrac{1}{2}\mathrm{Re}[-(p_1(y)\tilde{u}_1(y))_{x=L_1-} + (p_1(y)\tilde{u}_1(y))_{x=L_2+}] \quad (23)$$

$$w(y) = \frac{W(y)\cdot H}{\frac{1}{2}\int_{-H/2}^{H/2}\mathrm{Re}[-(p_1\tilde{u}_1)_{x=L_1-} + (p_1\tilde{u}_1)_{x=L_2+}]dy} \quad (24)$$

$$\eta_{st}(y) = \frac{w(y)}{q(y)} \quad (25)$$

where q is the local heat addition rate to the stack per its cross-sectional area, which can be found from the enthalpy flux along the stack pores [4] and conduction-type heat transfer. It is assumed that the heat conduction leak in the stack occurs mainly in the gas, and the stack solid plates have negligibly low longitudinal thermal conductivity. The normalized acoustic power density and the stack-based efficiency are calculated for the system defined above under the temperature difference $\Delta T = 100$ K and with variable width H. The results are shown in Fig. 7. The resonator with aspect ratio $H/L = 0.5$ has nearly uniform acoustic power flux and local efficiency, with the difference between values at the walls ($2y/H = \pm 1$) caused by the temperature variation along the *y*-axis. The acoustic pressure and velocity shown in Fig. 6 also have small asymmetry due to finite ΔT_y. In real systems this will also lead to asymmetry of the flexing wall velocity, which is assumed symmetrical in the present study (Eq. (21)).

The transverse nonuniformities become large at aspect ratio $H/L = 1.5$. They are caused by a strongly nonuniform acoustic field in the stack, such as the local increase of the imaginary velocity amplitude (similar to that in Fig. 6(*d*)). This variation across-the-stack suggests that optimized stacks in such systems should have lengths and positions of the stack segments varying over the resonator cross section.

The engine produces net acoustic power above the temperature difference threshold. Steady-state operations, i.e., when acoustic amplitudes are saturated and do not change in time, will require either nonlinear acoustic losses or limits on how much heat can be given/taken to/from the stack or how much acoustic power can be extracted from the wall oscillator. In this example, we consider the amount of extracted mechanical power to be the limiting factor. The thermomechanical efficiency in the excited regime can be defined as follows:

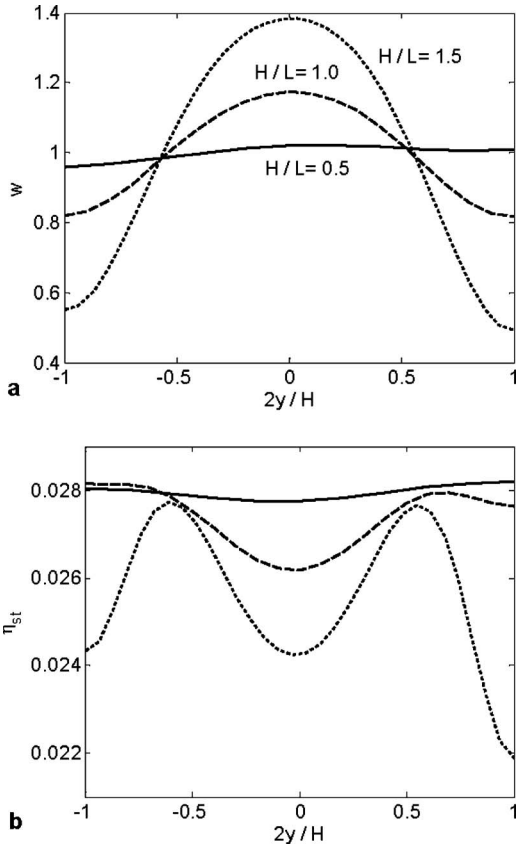

Fig. 7 (*a*) Normalized flux of acoustic power produced in the stack. (*b*) Local stack-based thermoacoustic efficiency. Solid line, $H/L = 0.5$; dashed line, $H/L = 1.0$; and dotted line, $H/L = 1.5$.

$$\eta_{tm} = \frac{P}{Q} \quad (26)$$

where P is the mechanical power removed from the oscillator (Eq. (15)) and Q is the rate of total heat supplied to the stack [4]. Calculated for the system with the same parameters defined above, the aspect ratio $H/L = 1.0$, and variable mechanical loads and stack temperature differences, the thermomechanical efficiency is shown in Fig. 8. Two low-power cases (0.1 W/m and 1.0

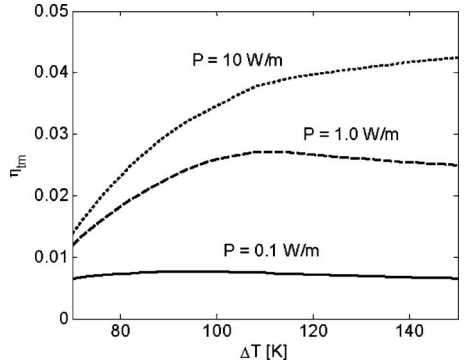

Fig. 8 Calculated thermomechanical efficiency. Solid line, $P = 0.1$ W/m; dashed line, $P = 1.0$ W/m; and dotted line, $P = 10$ W/m.

W/m) correspond to the relative acoustic pressure amplitudes p_1/p_m below 2%, while the highest power case (10 W/m) corresponds to p_1/p_m within 2–6% in the considered range of ΔT. Unaccounted here, finite-amplitude acoustic effects may become important in the case with the highest power output.

As shown in Fig. 8, the thermomechanical efficiency increases with the mechanical power output at fixed ΔT since the parasitic heat conduction along x-axis is not sensitive to the acoustic amplitudes, and the contribution of the heat leak to the total rate of supplied heat decreases with increasing power output (or acoustic amplitudes).

The dependence of efficiency on the stack temperature difference at fixed power output is not monotonic. If ΔT is only slightly greater than ΔT_{cr}, then the oscillator power-extracting coefficient R is small, and acoustic amplitudes must be large for a constant power level P (Eq. (15)). The supplied heat rate increases with both the acoustic amplitudes and the stack temperature difference [4]. With increasing ΔT, R also increases, while acoustic amplitudes must decrease to keep constant P. Therefore, the supplied heat rate initially decreases and the efficiency initially increases with increasing ΔT when the conduction heat leak is relatively small. At sufficiently large ΔT, the conduction heat leak becomes a dominant component of the supplied heat, leading to an increase of Q and a reduction of the efficiency. This suggests an existence of optimal ΔT at fixed P, where the efficiency reaches its maximum. The efficiency peak shifts to higher temperature differences at larger mechanical loads (Fig. 8).

It should be emphasized that heat transfer due to acoustic streaming is not accounted for here because only low amplitudes are considered. No optimization of the system geometry and material properties is attempted in this study. Hence, the efficiency and power in Fig. 8 correspond to realistic values in the chosen configuration, but significant improvements can be expected when the system parameters are designed for a specific operational condition. Nevertheless, even efficiency levels of several percent are considered attractive for practical applications of small-scale power systems [12]. At the same time, various nonlinear effects ignored here may negatively impact the system performance in high-amplitude regimes.

4 Conclusions

A numerical model has been developed for calculating low-amplitude acoustic fields in resonators with nonuniform media and boundary conditions. This method can be used for designing thermoacoustic devices and other systems where the assumption about one-dimensionality of pressure and mean temperature fields does not hold and acoustic losses at solid surfaces are important. The main advantage of the considered approach in comparison with complete thermoviscous modeling by computational fluid dynamics codes is the computational efficiency. Sparse numerical grids can be used in the bulk of resonators, while analytical solutions in boundary layers near solid surfaces provide appropriate boundary conditions. The model is convenient for optimizing thermoacoustic systems since all important parameters of geometry and material properties are included into consideration, and calculations are fast.

The example considered in this paper involves a new configuration of a small-scale thermoacoustic engine. Operating at a frequency much lower than a natural frequency of the acoustic resonator, such an engine may achieve reasonably high efficiencies and have a low temperature difference threshold in order to serve as a portable electric power source when the engine is coupled with an electroacoustic transformer.

Future modeling developments in the direction of this study can include a heat transfer analysis for determining a temperature field in the resonator at given thermal boundary conditions. Accounting for large-amplitude acoustic effects, such as acoustic streaming and higher harmonics, will be important for high-power regimes of operations of thermoacoustic engines. More detailed models for electroacoustic transformers are needed to adequately predict electric power generated at different electric loads and to provide accurate boundary conditions at the flexing walls of resonators. A complete validation of the developed model requires experimental studies of thermoacoustic resonators with significant transverse nonuniformities in the acoustic and temperature fields.

Acknowledgment

This material is based on the work supported by the National Science Foundation under Grant No. 0853171.

References

[1] Howe, M. S., 1998, *Acoustics of Fluid-Structure Interactions*, Cambridge University Press, Cambridge.
[2] Bossart, R., Joly, N., and Bruneau, M., 2003, "Hybrid Numerical and Analytical Solutions for Acoustic Boundary Problems in Thermo-Viscous Fluids," J. Sound Vib., **263**, pp. 69–84.
[3] Arnott, W. P., Bass, H. E., and Raspet, R., 1991, "General Formulation of Thermoacoustics for Stacks Having Arbitrarily Shaped Pore Cross Sections," J. Acoust. Soc. Am., **90**, pp. 3228–3237.
[4] Swift, G. W., 2002, *Thermoacoustics: A Unifying Perspective for Some Engines and Refrigerators*, ASA, Sewickley, PA.
[5] Ward, W. C., and Swift, G. W., 1994, "Design Environment for Low-Amplitude Thermoacoustic Engines," J. Acoust. Soc. Am., **95**, pp. 3671–3672.
[6] Symko, O. G., Abdel-Rahman, E., Kwon, Y. S., Emmi, M., and Behunin, R., 2004, "Design and Development of High Frequency Thermoacoustic Engines for Thermal Management in Microelectronics," Microelectron. J., **35**, pp. 185–191.
[7] Jung, S., and Matveev, K. I., 2010, "Study of Small-Scale Standing-Wave Thermoacoustic Engine," J. Mech. Eng. Sci., **224**, pp. 133–141.
[8] Swift, G. W., 1992, "Analysis and Performance of a Large Thermoacoustic Engine," J. Acoust. Soc. Am., **92**, pp. 1551–1563.
[9] Blackstock, D. T., 2000, *Fundamentals of Physical Acoustics*, Wiley, New York.
[10] Olson, J. R., and Swift, G. W., 1997, "Acoustic Streaming in Pulse Tube Refrigerators: Tapered Pulse Tubes," Cryogenics, **37**, pp. 769–776.
[11] Matveev, K. I., Swift, G. W., and Backhaus, S. N., 2006, "Temperatures Near the Interface Between an Ideal Heat Exchanger and a Thermal Buffer Tube or Pulse Tube," Int. J. Heat Mass Transfer, **49**, pp. 868–878.
[12] Epstein, A. H., 2004, "Millimeter-Scale, Micro-Electro-Mechanical Systems Gas Turbine Engines," ASME J. Eng. Gas Turbines Power, **126**, pp. 205–226.